รายงานวิจัย

การศึกษาปฏิกิริยาสมดุลโครงรูปและการเกิดสารประกอบเชิงซ้อนกับแคตไอออนของสารประกอบเซมิคาร์บาโซนและอนุพันธุ์

โดย

วิทยา เรืองพรวิสุทธิ์

กันยายน 2549

Chulalongkorn University

Rachadapiseksompoj Research Fund

Research Report

A Study of Conformational Equilibrium of Semicarbazone Derivatives and Their Complexes with Cations

by

Vithaya Ruangpornvisuti

September 2006

จุฬาลงกรณ์มหาวิทยาลัย

ทุนวิจัย
กองทุนรัชดาภิเษกสมโภช

รายงานผลการวิจัย

การศึกษาปฏิกิริยาสมดุลโครงรูปและการเกิดสารประกอบเชิงซ้อนกับแคตไอออนของสารประกอบ

เซมิคาร์บาโซนและอนุพันธุ์

โดย

วิทยา เรืองพรวิสุทธิ์

กันยายน 2549

ACKNOWLEDGEMENT

ชื่อโครงการ	การศึกษาปฏิกิริยาสมดุลโครงรูปและการเกิดสารประกอบเชิงซ้อนกับแคตไอออนของสารประกอบเซมิคาร์บาโซนและอนุพันธุ์
ชื่อผู้วิจัย	วิทยา เรืองพรวิสุทธิ์
เดือนและปีที่ทำวิจัยเสร็จ	กันยายน 2549

บทคัดย่อ

โครงสร้างของสารประกอบเซมิคาร์บาโซน picolinaldehyde N-oxide thiosemicarbazone (Hpiotsc), 2-benzoylpyridine semicarbazone (H2BzPS), ทอโทเมอร์ต่าง ๆ ที่เกี่ยวข้อง และสารประกอบเชิงซ้อนที่เกิดขึ้นกับโลหะ Ni(II), Cu(II) และ Zn(II) คำนวณได้โดยวิธีดีเอฟทีในระดับทฤษฎี B3LYP/LANL2DZ สมบัติเทอร์โมไดนามิกของปฏิกิริยาทอโทเมอไรเซชันของสารประกอบ Hpiotsc และ H2BzPS และการคำนวณปฏิกิริยาการเกิดสารประกอบเชิงซ้อนในระดับทฤษฎีเดียวกัน ตัวแปรทางโครงสร้างที่คำนวณได้ของสารประกอบเชิงซ้อน $[Ni(Hpiotsc)_2]^{2+}$, $[Cu(Hpiotsc).Cl_2]$ and $[Zn(Hpiotsc).Cl_2]$ มีค่าใกล้เคียงกับข้อมูลที่ได้จากเอกซ์เรย์ สารประกอบอนุพันธ์ของเซมิคาร์บาโซนชนิดเอริลได้ศึกษาเพื่อพัฒนาให้เป็นสารการฆ่าแบคทีเรีย โดยการหาความสัมพันธ์ระหว่างโครงสร้างกับฤทธิ์การฆ่าแบคทีเรีย ซึ่งเป็นการวิเคราะห์ที่เรียกว่าคิวเอสเออาร์ (QSAR) โดยพบว่าฤทธิ์การฆ่าแบคทีเรียขึ้นกับค่าไฮโดรโฟบิซิทีของสารประกอบเซมิคาร์บาโซนชนิดเอริลเป็นส่วนสำคัญ และ ขึ้นกับตัวแปรชี้วัดชนิดหมู่แทนที่ โดยมีการนำเสนอตัวแปรชี้วัดดัดแปลงตัวใหม่สำหรับการนำไปประยุกต์ใช้ในการวิเคราะห์คิวเอสเออาร์ในระบบสารประกอบที่คล้ายคลึงกัน

Project Title   A Study of Conformational Equilibrium of Semicarbazone Derivatives and Their Complexes with Cations

Name of investigator   Vithaya Ruangpornvisuti

Year   September 2006

Abstract

The structure optimizations of picolinaldehyde N-oxide thiosemicarbazone (Hpiotsc), 2-benzoylpyridine semicarbazone (H2BzPS), their imino tautomers and their complexes with Ni(II), Cu(II) and Zn(II) were carried out using DFT calculations at the B3LYP/LANL2DZ level of theory. Thermodynamic properties of tautomerizations of Hpiotsc and H2BzPS and complexations of their complexes derived from the frequency calculations at the same level were obtained. The B3LYP/LANL2DZ-optimized geometry parameters for the complexes of $[Ni(Hpiotsc)_2]^{2+}$, $[Cu(Hpiotsc).Cl_2]$ and $[Zn(Hpiotsc).Cl_2]$ show good agreement with their corresponding X-ray crystallographic data. Aryl semicarbazone derivatives have been studied for the development of new antituberculous agents. The quantitative structure activity relationship (QSAR) analysis for the antituberculous activity of the aryl semicarbazones were carried out in terms of the molecular hydrophobicity and indicator variables using the multiple linear regression method. The new definition for indicator variables based on the substituents of the aryl semicarbazones was proposed and employed in the QSAR analysis.

CONTENTS

LIST OF FIGURES

LIST OF TABLES

CHAPTER I

INTRODUCTION

1.1 Molecular structures and tautomerizations of 2-benzoylpyridine semicarbazone and picolinaldehyde N-oxide thiosemicarbazone and their complexations with Ni(II), Cu(II) and Zn(II)

Many carbazones of variously substituted benzaldehyde and acetophenone were studied on their IR spectroscopic properties [1]. Phenylthiosemicarbazone (HAPhTSC) and phenylsemicarbazone (HAPhSC) were investigated [2] for their activity in the maximal electroshock (MES) anticonvulsant screen, the subcutaneous pentylenetetrazole (scPTZ) test, neurotoxicity screens and other biological properties [3, 4]. Crystal structures of metal complexes with thiosemicarbazone derivatives were prepared and spectroscopically characterized [5,6]. Coordinations of thiosemicarbazone derivatives to form complexes with ruthenium [7–9], osmium [10], rhodium [11], and tin [12] were widely observed. The molecular structures of nickel complexes with thiosemicarbazone and semicarbazone ligands were prepared and characterized by IR spectroscopic and other measurements [13]. The thiosemicarbazone derivatives and their metal complexes have been widely of interest as antitumer, antibacterial, antiviral, antimalarial agents [14–23]. Single crystal of semicarbazone was grown and identified by X-ray diffraction, and its functional groups were identified using FT-IR spectrum [24].

Due to the semicarbazone derivatives being used to evaluate compounds for anticonvulsant activities and their metal complexes processing for wide range of biological activities including antibacterial, antimalarial and antineoplastic effects, their structural information should be very useful for pharmaceutical purpose. The previous work, the molecular structures of 2-formylpiridine, 3-formylpiridine and 4-formylpiridine semicarbazone complexes with Co(II), Ni(II) and Zn(II), and reaction

energies were studied using DFT method [25]. In the present work, the structures of the complexes of picolinaldehyde N-oxide thiosemicarbazone (Hpiotsc) and 2-benzoylpyridine semicarbazone (H2BzPS), as shown in Figure 1.1, with Ni(II), Cu(II) and Zn(II) have been optimized using DFT/B3LYP/LANL2DZ method. The X-ray crystallographic structures of these complexes have been compared with their corresponding B3LYP/LANL2DZoptimized structures. Reaction energies and thermodynamic properties of their complexation have been computed at the B3LYP/LANL2DZ level with the zero-point vibrational energy corrections. The similar manner of methodology using on the systems of HMPAO/Zinc [26], BHam/technetium [27], and *N,N'*-propylene bis(benzohydroxamamide) complexes with oxotechnetium(V), and oxorhenium(V) [28] has been applied in this present work.
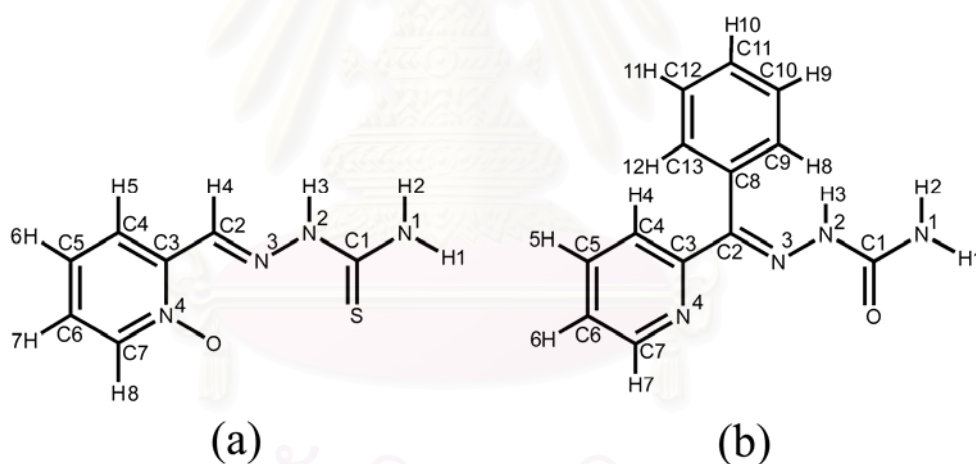
Figure 1.1 General structures of (a) H2BzPS and (b) Hpiotsc.

1.2 Aryl semicarbazone derivatives as anti-mycobacterium tuberculous agent

Tuberculosis (TB) is a serious health problem worldwide [29] and one of the most common infectious diseases known to man [30]. It causes more than two million deaths due to its infection [31].   The emergence of drug-resistant strains of

Mycobacterium tuberculosis leads to the need for developing new chemotherapeutic agents [32]. TB is a cofactor in the progression of the decease with human immunodeficiency virus (HIV). There were approximately 10 million adults who were infected with both TB and HIV. Recently, a 3D-QSAR analysis of ring-substituted quinolines with anti-tuberculosis activity have been carried out by three different methods [33]. Aryl substituted semicarbazones were synthesized [34] and tested for their anti-mycobacterials potency [35]. The potent anti-tuberculosis compounds exhibiting activity a drug-sensitive strain of *Mycobacterium tuberculosis* H37Rv [36-38]. A new semicarbazone derivative of curcumin was synthesized and exam for antioxidant, antiproliferative and antiradical activities [39]. In the previous work, the conformational structures of semicarbazone and thiosemicarbazone derivatives investigated in terms of their tautomerization and interconversion reactions were carried out by quantum chemical methods [25, 40]. As Hansch has been considered QSAR research as a major tool in drug discovery, a SQAR approach has been widely employed to explore the ligand and enzyme interactions [32-43].

In the present work, we are in attempt to explore the quantitative structure-activity relationship of the aryl semicarbazones as anti-mycobacterium tuberculous agent. We used a multiple linear regression (MLR) for modeling the observed anti-mycobacterium tuberculous activity of 10 aryl semicarbazone derivatives as shown in Figure 1.2. The indicator variables based on the substituents of the aryl semicarbazones have been firstly defined and employed to analyze for the best accurate QSAR model.
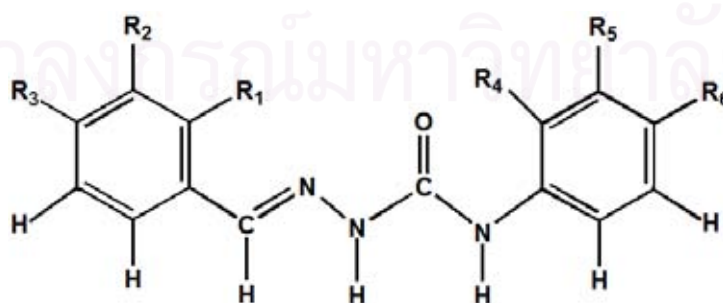
Figure 1.2 General structure of the aryl semicarbazone.

CHAPTER II

Theories and Methodologies

2.1 Quantum chemical methods

2.1.1 Semi-empirical Methods

Semi-empirical quantum chemistry methods are based on the Hartree-Fock formalism, but make many approximations and obtain some parameters from empirical data. They are very important in computational chemistry for treating large molecules where the full Hartree-Fock method without the approximations is too expensive. The use of empirical parameters appears to allow some inclusion of correlation effects into the methods.

2.1.1.1 AM1 Method

AM1, Austin Model 1 [44], was modified from MNDO (Modified Neglect of Diatomic Overlap) method and became clear that there were certain systematic errors. For example the repulsion between two atoms which are 2-3 Å apart is too high. This has as a consequence that activation energies in general are too large. The source was traced to too repulsive an interaction in the core-core potential. To remedy this, the core-core function was modified by adding Gaussian functions, and the whole model was reparameterized. The core-core repulsion of AM1 has the form

$$V_{nn}(A,B) = V_{nn}^{MINDO}(A,B) + \frac{Z_A^{'} Z_B^{'}}{R_{AB}} X (\sum_k a_{kA} e^{-b_{kA}(R_{AB}-c_{kA})^2} + \sum_k a_{kB} e^{-b_{kB}(R_{AB}-c_{kB})^2})$$

$$(2.1)$$

Where k is between 2 and 4 depending on the atom. It should be note that the Gaussian functions more or less were added as patches onto the underlying parameters, which explains why different number of Guassians are used for each

atom. As with MINDO, the G_{ss}, G_{sp}, G_{pp}, G_{p2}, H_{sp} parameters are taken from atomic spectra, while the rest including the a_k, b_k and c_k constants, are fitted to molecular data.

2.1.1.2 PM3 Method

PM3 is a short name of MNDO-PM3 (Modified Neglect of Diatomic Overlap, Parametric Method Number 3) [45]. PM3 is a method of the optimization process automatic, by deriving and implementing formulas for the derivative of a suitable error function with respect to the parameters. All parameters could then be optimized simultaneously, including the two-electron terms, and a significantly larger trianing set with several hundred data could be employed. In this reparameterization, the AM1 expression for the core-core repulsion was kept, except that only 2 Gaussians were assigned to each atom. These Gaussian parameters were included as an integral part of the model, and allowed to vary freely.

2.1.2 Density Functional Theory (DFT) Methods

DFT is a quantum mechanical method used in physics and chemistry to investigate the electronic structure of many-body systems, in particular molecules and the condensed phases. DFT is among the most popular and versatile methods available in condensed matter physics and computational chemistry. A popular functional is known as BLYP (Becke, Lee, Yang and Parr) [46-48]. Even more widely used is B3LYP which is a hybrid method in which the DFT exchange functional, in this case from BLYP, is combined with the exact exchange functional from Hartree-Fock theory.

2.1.2.1 Basis Set

A basis set is the mathematical description of the orbitals within a system (which in turn combine to approximate the total electronic wavefunction) used to perform the theoretical calculation. Larger basis sets more accurately approximate the orbitals by

imposing fewer restrictions on the locations of the electrons in space. In the quantum mechanical picture, electrons have a finite probability of existing anywhere in space; this limit corresponds to the infinite basis set. Standard basis sets for electronic structure calculations use linear combinations of gaussian functions to form the orbitals. Gaussain (program) offers a wide range of per-defined basis sets, which may be classified by the number and types of basis functions that they contain. Basis sets assign a group of basis functions to each atom within a molecule to approximate its orbitals. These basis functions themselves are composed of a linear combination of gaussian functions; such basis functions are referred to as contracted functions, and the component gaussian functions are referred to as primitives. A basis function consisting of a single gaussian function is termed uncontracted.

2.1.2.2 Minimal basis Set

Minimal basis sets contain the minimum number of basis functions needed for each atom, as in these examples:

$$H : 1s$$

$$C : 1s, 2s, 2p_x, 2p_y, 2p_z$$

Minimal basis sets use fixed-size atomic-type orbitals. The STO-3G basis set is a minimal basis set (although it is not the smallest possible basis set). It uses three gaussian primitives per basis function, which accounts for the "3G" in its name. "STO" stands for "Slater-type orbitals," and the STO-3 basis set approximates Slater orbitals with gaussian functions.

2.1.2.3 Split valence basis Set

The first way that a basis set can be made larger is to increase the number of basis functions per atom. Split valence basis sets, such as 3-21G and 6-31G, have two (or more) sizes of basis function for each valence orbital. For example, hydrogen and carbon are represented as:

H : 1s, 1s'

C : 1s, 2s, 2s', $2p_x$, $2p_x$', $2p_y$, $2p_y$',$2p_z$,$2p_z$'

Where the primed and umprimed orbtals differ in size. The double zeta basis sets, such as the Dunning-Huzinage basis set (D95), form all molecular orbitals from linear combinations of two sizes of functions for each atomic orbital. Similarly, triple split valence basis sets, like 6-311G, use three sizes of contracted functions for each orbital-type.

2.1.2.4 Polarized basis Set

Split valence basis sets allow orbitals to change site, but not of change shape. Polarized basis sets remove this limitation by adding orbitals with angular momentum beyond what is required for the ground state to the description of each atom. For example, polarized basis sets add d functions to carbon atoms and f functions to transition metals, and some add p functions to hydrogen atoms. So far, the only polarized basis set we've used is 6-31G(d). Its name indicates that it is the 6-31G basis set with d functions added to heavy atoms. This basis set is becoming very common for calculations involving up to medium-sized systems. This basis set is also known as 6-31G*. Another popular polarized basis set is 6-31G(d,p), also known as 6-31G**, which adds p functions to hydrogen atoms in addition to the d functions on heavy atoms.

2.1.2.5 Diffuse functions

Diffuse functions are large-size versions of s- and p-type functions (as oppose to the standard valence-size functions). They allow orbitals to occupy a larger region of space. Basis sets with diffuse functions are important for systems where electrons are relatively far from the nucleus: molecules with lone pairs, anions and other systems with significant negative charge, systems in their excited states, systems with low ionization potentials, descriptions of absolute acidities, and so on. The 6-31+G(d) basis set is the 6-31G(d) basis set with diffuse functions added to heavy atoms. The

double plus version, 6-31++G(d), adds diffuse functions to the hydrogen atoms as well. Diffuse functions on hydrogen atoms seldom make a significant difference in accuracy.

2.1.2.6 Effective Core Potential (ECP)

In effective core potential (ECP) basis sets, the core-electrons are replaced by an effective nuclear charge which greatly improves computational efficiency. The effective core approximation includes relativistic contributions which become noticeable for heavy elements (Hg, Au, Pt, etc.). This means that e.g. a calculation of a gold compound with the SDD basis set reproduces relativistic effects without using an explicit relativistic calculation (Dirac operator instead of Hamilton operator. The LANL2DZ [49-51] was developed in the Los Alamos National Laboratories (LANL), 2 is the version number and DZ indicates that it is a "double-zeta" basis set. There is no general nomenclature for basis sets. SDD stands for Stuttgart-Dresden, the cities of the inventors. All three basis sets give comparable results although the most recent one (SDD) is slightly superior and has largely replaced the LANL2DZ and CEP-121 basis sets.

2.2 Solvent effects

Tomasi's Polarized Continuum Model (PCM) is a cavity defined as a series of overlapping spheres and a numerical reaction field. The CPCM (COSMO) and IEFPCM facilities of Tomasi and coworkers are very useful methods for studying molecules in solution and predicting solvent effects.

2.2.1 CPCM Model

The conductor-like polarizable continuum model (CPCM) [52] using several cavity models developed in the framework of the polarizable continuum model (PCM), has been reformulated and newly implemented in order to compute energies, geometric

structures, harmonic frequencies, and electronic properties in solution for any chemical system.

2.2.2 IEFPCM Model

The solvation model known as Integral-Equation-Formalism Polarizable Continuum Model (IEFPCM) [53] has been originally developed in collaboration with Dr. Eric Cances. The approach followed is based on the partition of the whole system into two subsytems, the molecule(s) under scrutiny ("the solute") and the "environment". This latter is treated as a macroscopic and continuous medium characterized by some specific macroscopic physical properties, in particular its dielectric permittivity. By contrast, the solute is described at a microscopic level (usually using a quantum-mechanical description) and it is assumed to be immersed in the continuum, or better in a cavity of proper shape and dimension. The cavity which is built according to the real geometric structure of the target solute univocally defines the closed surface which separates the solute and the solvent, and, at the same time, it is used to formulate the basic electrostatic equations characterizing the solute-solvent interactions.

CHAPTER III

EXPERMENTAL

3.1 Computational methods

Geometrical structures of studied compounds were carried out using the Becke's threeparameter exchange functional with the Lee–Yang–Parr correlation functional (B3LYP) [46–48] using the Los Alamos LANL2DZ split-valence basis set [49–51]. The electronic ground states of the singlet state was used in the DFT calculations for all studied compounds except for all copper complexes, the ground doublet state was used. DFT calculations were performed with the zero-point vibrational energy corrections. Vibrational analyses have been carried out on the minima. All computations were performed with the GAUSSIAN 03 program [54]. The molecular graphics of all studied molecules were generated with the MOLEKEL 4.3 program [55].

The Mulliken electronegativity (χ), chemical hardness (η), and electronic chemical potential (μ) for all isomers of the nitrosamines were computed using orbital energies of the highest occupied molecular orbital (HOMO) and the lowest unoccupied molecular orbital (LUMO) at the B3LYP/LANL2DZ level of theory. The chemical hardness, electronic chemical potential and Mulliken electronegativity were derived from the first ionization potential (I) and electron affinity (A) of the N-electron molecular system with a total energy (E) and external potential ($\nu(\vec{r})$) using the relations: $\chi = -\left(\dfrac{\partial E}{\partial N}\right)_{\nu(\vec{r})} = -\mu \cong \dfrac{1}{2}(I + A)$ and $\eta = -\left(\dfrac{\partial E}{\partial N^2}\right)_{\nu(\vec{r})} \cong \dfrac{1}{2}(I - A)$, and the first ionization potential and electron affinity are $I = E(N-1) - E(N)$ and $A = E(N) - E(N+1)$ [56]. According to the Koopmans theorem [57], I and A were computed from the HOMO and LUMO energies using the relations: $I = -E_{HOMO}$ and $A = -E_{LUMO}$.

The standard enthalpy ΔH_{298}^O and Gibbs free energy changes ΔG_{298}^O of interconversion reactions have been derived from the frequency calculations. The rate constant k(T) derived from transition-state theory was computed from Gibbs free energy of activation $\Delta^\ddagger G_{298}^O$, using $k(T) = \dfrac{k_B T}{hc^O} e^{-\Delta^\ddagger G/RT}$, where c^O factor is assigned to unity [58] as applied in the previous works [25, 27-28, 59]. The equilibrium constant K at 298.15 K and one atmosphere is computed using a thermodynamic equation $\Delta G^O = -RT \ln K$.

3.2 Material and methods

3.2.1 Activity and biological data

The aryl semicarbazone derivatives investigated in this work are compounds **1A**, **1A'**, **1B**, **1C**, **1D**, **1E**, **2A**, **2B**, **2C**, **2D** and **2E**. In the QSAR study, the activities of compounds (**1A**, **1A'**, **1B**, **1C**, **1D**, **1E**, **2A**, **2B**, **2C**, **2D** and **2E**) measured in vitro against Mycobacterium tuberculosis strain H37Rv (ATCC 27294) in BACTEC 12B medium are obtained from the Reference 3. The parent molecule of these aryl semicarbazones, **3** and theoretical modeled molecules **4A**, **4B**, **4C**, **4D** and **4E** as shown in Figure 3.1 were used to examine for prediction of high activity molecules. The activities of these compounds (**1A**, **1B**, **1C**, **1D**, **1E**, **2A**, **2B**, **2C**, **2D** and **2E**) obtained from the Reference 35 were transformed using Equation 3.1 [67].

Activity (A) = − Log c + Log [% inhibition/(100 − % inhibition)],   (3.1)

where c is the molar concentration which is the product of (concentration in mg/mL) and (0.001)/(molecular weight).

3.2.2 Descriptors

As the performance of QSAR models depends mostly on the parameters used to rationalize the molecular structures, a set of descriptors related to physicochemical, electronic, geometric properties and indicator variables of the molecules was used. All descriptors were calculated based on the substituents R_1, R_2, R_3, R_4, R_5 and R_6 of the aryl semicarbazones of which general structure is shown in Figure 1.2.

The molecular properties of the aryl semicarbazone derivatives based on the semiempirical AM1 [43] method were computed with the HyperChem 7.0 program [60]. The initial structures of all the compounds were constructed using the Chem3D [61] and CAChe [62] programs. The AM1-optimized structures of all the aryl semicarbazone derivatives performed with the Gaussian 03 [54] are shown in Figure 3.1.

The QSAR properties used for each substituent are partial charges, surface area, volume, hydration energy, Log P, molecular refractivity (MR), polarizability and molecular weight (MW). The hydrophobic coefficient, Log P mostly suggested to be correlated with many biological activities [63-65] is the most effective descriptor. The indicator variables I_1, I_2, I_3 and I_4 used in this work are defined according to the activities of the compounds as the following descriptions.

I_1 is a value based on the R_1, R_2 and R_3 substituents which are replaced by NO_2 group and defined as 1, 3 and 2 for R_1, R_2 and R_3 substituents, respectively otherwise 0.

I_2 is a value based on the R_4 and R_5 substituents which are both replaced by CH_3 and Cl substituents and defined as 0 otherwise 1.

I_3 is defined as a value of 1 for single substitution of $NHCOCH_3$ for R_6.

I_4 is defined as $\dfrac{5}{2}I_1 + I_2 + 2 I_3$. This variable is a combination of all dependent indicator variables I_1, I_2 and I_3 as $I_4 = \sum\limits_{i=1}^{3} d_i I_i$, where as $d_1 = \dfrac{5}{2}$, $d_2 = 1$ and $d_3 = 2$.

3.2.3 Regression analysis

The multiple linear regression (MLR) method was employed to generate linear models between the antituberculous activity and the molecular descriptors. The quality of the model was considered as statistically satisfactory on the basis of squared correlation (r^2), correlation coefficient (r), standard deviation (s) and F-ratio (F). The regression models with a correlation coefficient larger than 0.80 were accepted as inter-correlated data.
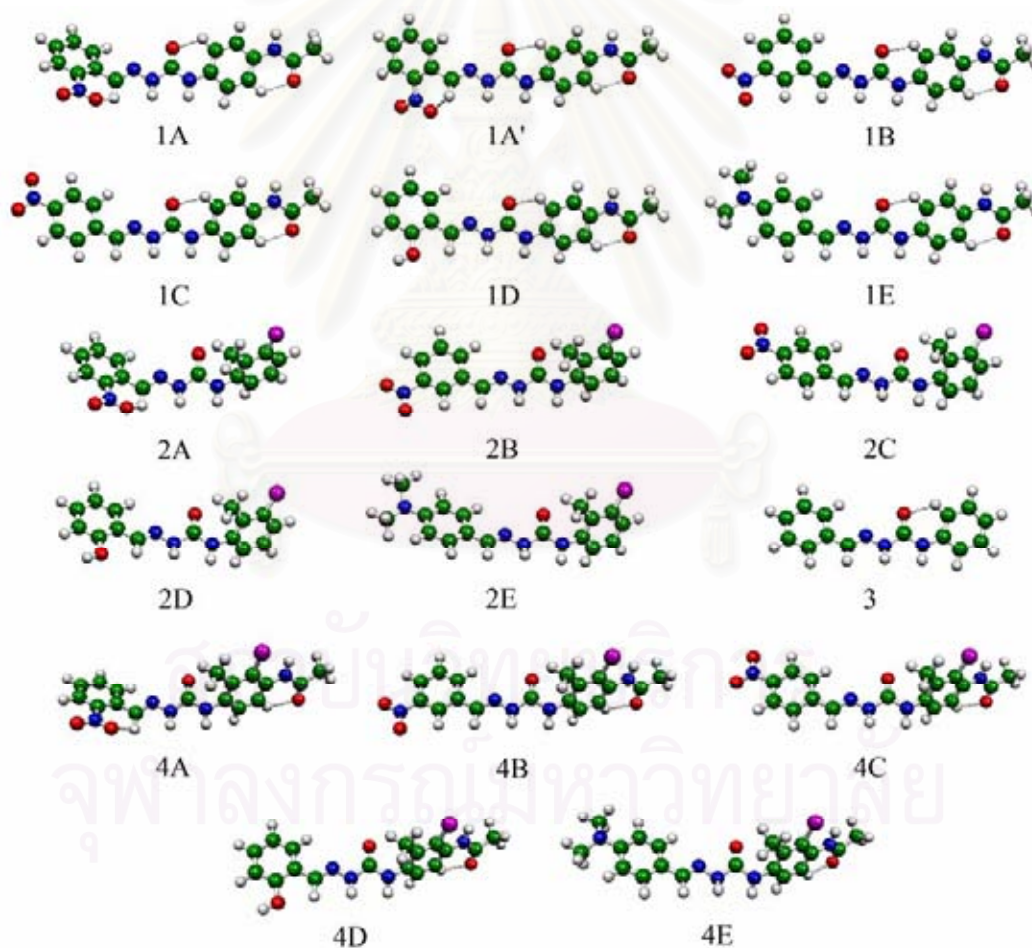
Figure 3.1 The AM1-optimized structures of the aryl semicarbazones.

CHAPTER IV

RESULTS AND DISCUSSION

4.1. Tautomerization of Hpiotsc and H2BzPS

The geometry optimizations of the picolinaldehyde N-oxide thiosemicarbazone, Hpiotsc and 2-benzoylpyridine semicarbazone, H2BzPS and their imino tautomers were carried out at the B3LYP/LANL2DZ level of theory. The energy profile for tautomerizations of the Hpiotsc and H2BzPS are shown in Figure 4.1(a) and 4.1(b), respectively. Rate constants of their tautomerizations in gas phase and aqueous phase evaluated via transition-state theory using their activation free energies, $\Delta^{\ddagger}G^{O}_{298}$ and equilibrium constants of their tautomerizations evaluated from their reaction free energies, ΔG^{O}_{298} are shown in Table 4.1. Activation energies due to the aqueous system as either IEFPCM or CPCM models are higher than that energies in gas-phase by approximate 10 kcal/mol for Hpiotsc system and ~ 6 kcal/mol for H2BzPS system. The activation free energies in both aqueous models (IEFPCM and CPCM) of tautomerizations for the systems of Hpiotsc and H2BzPS are hardly ever different. Both tautomerizations for Hpiotsc and H2BzPS systems are endothermic and non-spontaneous reactions. The atomic charges due to natural bond order, NBO and Mulliken population analysis, in unit of electrons, for the Hpiotsc and H2BzPS are shown in Table 4.2.

Energies of the highest occupied molecular orbital, E_{HOMO} and the lowest unoccupied molecular orbital, E_{LUMO} and frontier molecular orbital energy gap, $\Delta E_{\text{HOMO-LUMO}}$ of the Hpiotsc and H2BzPS and their imino tautomers computed at the B3LYP/LANL2DZ level of theory and their Mulliken electronegativities, chemical hardnesses, and electronic chemical potentials are shown in Table 4.3

Table 4.1 Equilibrium and rate constants of tautomerizations of the picolinaldehyde N-oxide thiosemicarbazone (Hpiotsc, $\mathbf{L^1}$) and 2-benzoylpyridine semicarbazone (H2BzPS, $\mathbf{L^2}$) and their energies, computed at the B3LYP/LANL2DZ level of theory

Reactions / systems	$\Delta^{\ddagger}E$ [a,b]	$\Delta^{\ddagger}G$ [a,c]	$\Delta\Delta^{\ddagger}G$ [a,d]	k_{298} [e]	k_{298} [d,e]	ΔE [a,b]	ΔH [a,c]	ΔG [a,c]	$\Delta\Delta G$ [a,d]	K_{298}	K_{298} [d]
In water, IEFPCM model											
$\mathbf{L^1} \rightarrow$ TS1 $\rightarrow \mathbf{L^{1\prime}}$	49.07	49.09	49.74	6.38×10^{-24}	2.15×10^{-24}	25.68	25.29	26.24	29.40	4.93×10^{-20}	2.36×10^{-22}
$\mathbf{L^2} \rightarrow$ TS2 $\rightarrow \mathbf{L^{2\prime}}$	53.88	55.55	50.81	1.18×10^{-28}	3.52×10^{-25}	21.32	20.26	23.97	22.28	2.34×10^{-18}	4.06×10^{-17}
In water, CPCM model											
$\mathbf{L^1} \rightarrow$ TS1 $\rightarrow \mathbf{L^{1\prime}}$	49.16	48.17	49.83	5.55×10^{-24}	1.84×10^{-24}	25.74	25.36	26.29	29.47	4.55×10^{-20}	2.09×10^{-22}
$\mathbf{L^2} \rightarrow$ TS2 $\rightarrow \mathbf{L^{2\prime}}$	53.94	53.14	50.85	6.90×10^{-27}	3.26×10^{-25}	21.30	20.83	21.45	2.26	1.65×10^{-16}	4.19×10^{-17}
In gas-phase, direct proton transfer											
$\mathbf{L^1} \rightarrow$ TS1 $\rightarrow \mathbf{L^{1\prime}}$	39.43	38.46	- [f]	3.96×10^{-16}	- [f]	19.54	20.04	18.55	- [f]	2.25×10^{-14}	- [f]
$\mathbf{L^2} \rightarrow$ TS2 $\rightarrow \mathbf{L^{2\prime}}$	47.10	47.37	- [f]	1.66×10^{-22}	- [f]	20.92	20.79	21.08	- [f]	3.11×10^{-16}	- [f]

[a] In kcal mol^{-1}.

[b] Total energy with zero-point energy corrections.

[c] Frequency calculations at the B3LYP/LANL2DZ level.

[d] In aqueous solution, derived from the single-point PCM-model calculations ($\varepsilon = 78.4$) at the B3LYP/LANL2DZ level.

[e] In s^{-1}.

[f] Undeterminable.

[g] No computation is performed.

Table 4.2 Atomic charges (in e) for the picolinaldehyde N-oxide thiosemicarbazone (Hpiotsc) and 2-benzoylpyridine semicarbazone (H2BzPS)

Hpiotsc			H2BzPS		
Atoms [a]	Mulliken	NBO	Atoms [b]	Mulliken	NBO
O	-0.322	-0.448	O	-0.289	-0.551
S	-0.032	-0.160	N1	-0.549	-0.894
N1	-0.581	-0.845	N2	-0.398	-0.480
N2	-0.313	-0.442	N3	0.014	-0.227
N3	0.142	-0.174	N4	-0.181	-0.568
N4	-0.003	0.019	C1	0.306	0.853
C1	-0.071	0.261	C2	-0.022	0.170
C2	-0.327	0.002	C3	0.123	0.182
C3	0.328	0.139	C4	-0.278	-0.228
C4	-0.264	-0.212	C5	-0.193	-0.173
C5	-0.224	-0.226	C6	-0.164	-0.249
C6	-0.140	-0.229	C7	-0.341	0.077
C7	-0.248	0.016	C8	0.331	-0.063
H1	0.350	0.437	C9	-0.362	-0.180
H2	0.296	0.397	C10	-0.223	-0.208
H3	0.253	0.365	C11	-0.234	-0.215
			C12	-0.227	-0.213
			C13	-0.388	-0.226
			H1	0.339	0.426
			H2	0.208	0.405
			H3	0.374	0.427

[a] Atomic numbering is shown in Figure 2(a). [b] Atomic numbering is shown in Figure 2(b).

Table 4.3 The E_{LUMO} and E_{HOMO} energies and frontier molecular orbital energy gap, $\Delta E_{HOMO-LUMO}$ of the picolinaldehyde N-oxide thiosemicarbazone (Hpiotsc, $\mathbf{L}^1$) and 2-benzoyl pyridine semicarbazone (H2BzPS, $\mathbf{L}^2$) and their imino tautomers computed at the B3LYP/LANL2DZ level of theory

Compounds/isomers	p [a]	E_{LUMO} [b]	E_{HOMO} [b]	$\Delta E_{HOMO-LUMO}$ [b]	η [b, c]	μ [b, d]	χ [b, e]
$\mathbf{L}^1$	9.475	-2.20	-5.33	3.13	1.56	-3.77	3.77
TS1	9.182	-2.37	-5.93	3.56	1.78	-4.15	4.15
$\mathbf{L}^1_i$	7.625	-2.23	-5.90	3.67	1.84	-4.07	4.07
$\mathbf{L}^2$	10.921	-2.01	-6.07	4.05	2.03	-4.04	4.04
TS2	11.058	-2.18	-7.89	5.71	2.86	-5.03	5.03
$\mathbf{L}^2_i$	8.246	-1.99	-5.93	3.95	1.97	-3.96	3.96

[a] In debye. [b] In eV. [c] Chemical hardness, $\eta = \Delta E_{HOMO-LUMO}/2$.

[d] Electronic chemical potential, $\mu = (E_{HOMO} + E_{LUMO})/2$.

[e] The Mulliken electronegativity, $\chi = -(E_{HOMO} + E_{LUMO})/2$.
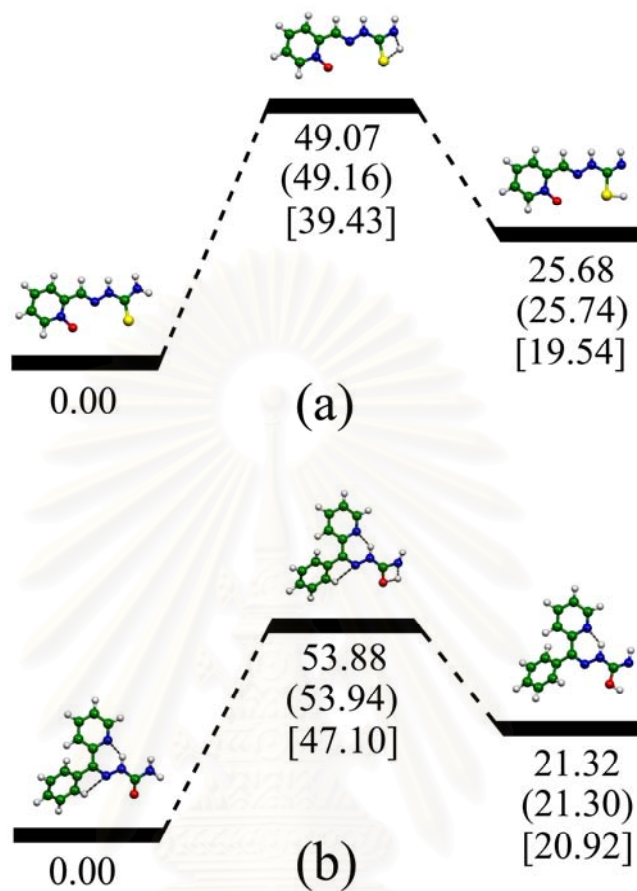
Figure 4.1 The energy profile for tautomerization reactions of (a) the Hpiotsc and (b) H2BzPS. Energies in water IEFPCM model, CPCM model (in parenthesis) and in gas phase (in bracket), in kcal/mol.
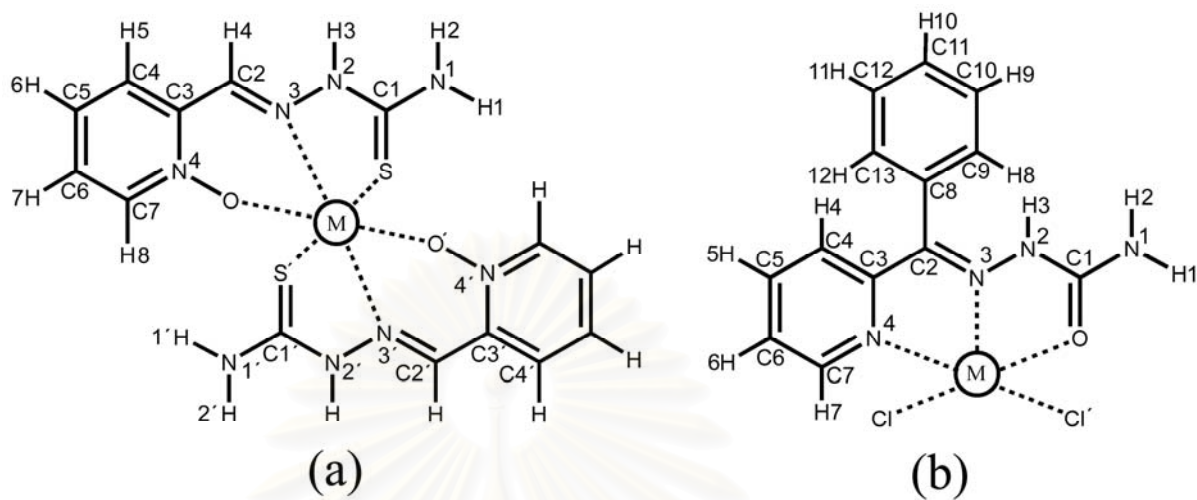
Figure 4.2 Atomic numbering for (a) the complexes of picolinaldehyde N-oxide thiosemicarbazone (Hpiotsc, $\mathbf{L}^1$) and (b) of 2-benzoyl pyridine semicarbazone (H2BzPS, $\mathbf{L}^2$) with M=Ni(II), Cu(II) and Zn(II).

4.2 Complexes of Hpiotsc and H2BzPS

The geometry optimizations of the Hpiotsc, H2BzPS, their imino tautomers and their complexes with Ni(II), Cu(II) and Zn(II) were carried out at the B3LYP/LANL2DZ level of theory. The B3LYP/LANL2DZ-optimized geometrical data for the Hpiotsc complexes with Ni(II), Cu(II) and Zn(II) in forms of $[Ni(HPiotsc)_2]^{2+}$, $[Cu(HPiotsc)_2]^{2+}$ and $[Zn(HPiotsc)_2]^{2+}$ are listed in Table 4.4. Atomic numbering for geometrical data of all studied complexes is illustrated in Figure 2. The B3LYP/LANL2DZ-optimized structures of complexes $[Ni(HPiotsc)_2]^{2+}$, $[Cu(HPiotsc)_2]^{2+}$, and $[Zn(HPiotsc)_2]^{2+}$ are shown in Figure 4.3. For the B3LYP/LANL2DZ-optimized geometrical data for the H2BzPS complexes as $[Ni(H2BzPS)]^{2+}$, $[Ni(H2BzPS.Cl_2)]$, $[Cu(H2BzPS)]^{2+}$, $[Cu(H2BzPS.Cl_2)]$, $[Zn(H2BzPS)]^{2+}$ and $[Zn(H2BzPS.Cl_2)]$ are listed in Table 4.5 and their geometrical structures are shown in Figure 4.4.

Reaction energies and thermodynamic properties of the complexations of Hpiotsc (L^1) and H2BzPS (L^2) with Ni(II), Cu(II) and Zn(II) are shown in Table 4.6. Relative stabilities for HPiotsc complexes are in decreasing order: $[Ni(HPiotsc)_2]^{2+}$ > $[Cu(HPiotsc)_2]^{2+}$ > $[Zn(HPiotsc)_2]^{2+}$ and for complexes $ML^{2\ 2+}$ and ML^2Cl_2 are in decreasing orders: $NiL^{2\ 2+}$ > $CuL^{2\ 2+}$ >> $ZnL^{2\ 2+}$ and NiL^2Cl_2 > CuL^2Cl_2 > ZnL^2Cl_2, respectively. All the complexations are exothermic reaction and spontaneous process.
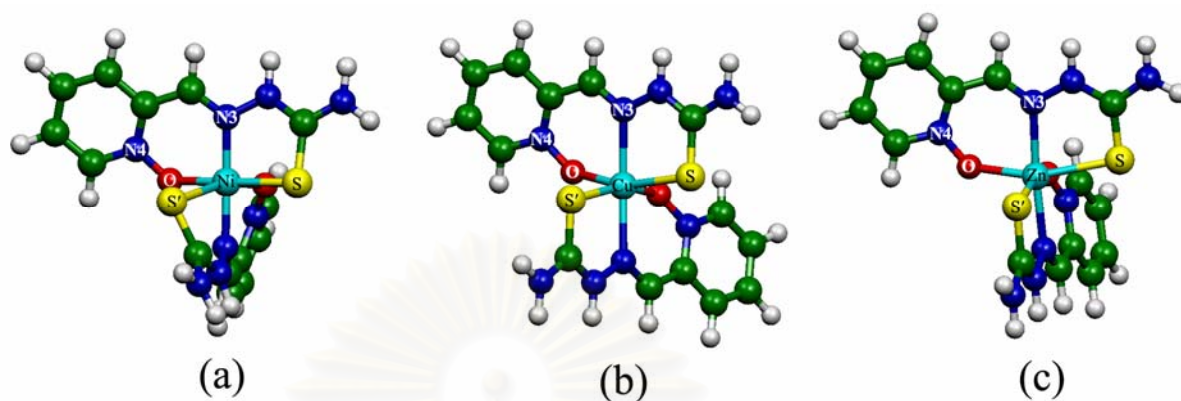
Figure 4.3 The B3LYP/LANL2DZ-optimized geometrical structures of complexes (a) [Ni(HPiotsc)$_2$]$^{2+}$, (b) [Cu(HPiotsc)$_2$]$^{2+}$ and (c) [Zn(HPiotsc)$_2$]$^{2+}$.

Figure 4.4 The B3LYP/LANL2DZ-optimized geometrical structures of complexes (a) [Ni(H2BzPS)]$^{2+}$ and [Ni(H2BzPS).Cl$_2$], (b) [Cu(H2BzPS)]$^{2+}$ and [Cu(H2BzPS).Cl$_2$], (c) [Zn(H2BzPS)]$^{2+}$ and [Zn(H2BzPS).Cl$_2$], above and below respectively.

สถาบันวิทยบริการ

จุฬาลงกรณ์มหาวิทยาลัย

Table 4.4 The B3LYP/LANL2DZ-optimized geometrical data for picolinaldehyde N-oxide thiosemicarbazone (Hpiotsc) complexes with Ni(II), Cu(I) and Zn(II)

Parameters [a]	$[Ni(HPiotsc)_2]^{2+}$		$[Cu(HPiotsc)_2]^{2+}$	$[Zn(HPiotsc)_2]^{2+}$
	Calculated	Experimental [b]	Calculated	Calculated
Bond length (Å)				
H1–N1	1.01	0.86	1.01	1.01
C1–N1	1.35	1.32	1.35	1.35
C1–S	1.75	1.69	1.75	1.74
C1–N2	1.38	1.35	1.38	1.39
N2–N3	1.39	1.37	1.38	1.39
C2–N3	1.31	1.28	1.31	1.31
C2–C3	1.45	1.45	1.46	1.46
C3–N4	1.38	1.36	1.39	1.39
N4–O	1.36	1.33	1.36	1.35
O–M	1.95	2.04	2.04	2.05
S–M	2.32	2.38	2.46	2.61
Bond angles				
H1–N1–C1	119.24	120.05	119.01	118.49
N1–C1–S	122.45	122.53	120.23	121.12
S–C1–N2	119.60	122.31	123.59	123.70
C1–N2–N3	119.40	120.87	120.80	122.37
N2–N3–C2	117.53	115.74	117.90	116.32
N3–C2–C3	126.27	126.64	125.95	127.95
C2–C3–C4	119.38	117.93	117.92	118.14
C2–C3–N4	122.13	123.46	123.82	123.58
C3–N4–O	121.96	123.11	123.34	122.42
N4–O–M	123.05	127.51	130.58	135.03
O–M–O′	86.78	79.69	82.55	88.37
S–M–S′	96.76	97.63	96.23	94.77
Dihedral angle (°)				
H1–N1–C1–S	1.95	-0.03	-0.30	-0.60
H1–N1–C1–N2	-178.49	179.99	178.70	178.85
N1–C1–N2–N3	-177.67	-177.28	-179.88	179.36
C1–N2–N3–C2	168.21	178.64	173.43	175.13
N2–N3–C2–C3	-178.92	-175.00	-177.71	-179.32
N3–C2–C3–C4	166.01	169.13	169.65	174.38
N3–C2–C3–N4	-13.88	-9.90	-10.16	-5.95
C2–C3–N4–O	-4.64	-6.23	-5.58	-1.90
C3–N4–O–M	31.95	25.69	34.18	20.63

[a] M= Ni^{2+}, Cu^{2+} and Zn^{2+}. [b] X-ray crystallographic data was taken from reference [66].

Table 4.5 The B3LYP/LANL2DZ-optimized geometrical data for 2-benzoylpyridine semicarbazone (H2BzPS) complexes with Ni(II), Cu(I) and Zn(II)

Parameters [a]	Ni(H2BzPS)]²⁺	[Ni(H2BzPS.Cl₂)]	[Cu(H2BzPS)]²⁺	[Cu(H2BzPS.Cl₂)]		[Zn(H2BzPS)]²⁺	[Zn(H2BzPS.Cl₂)]	
	Comp	Comp	Comp	Comp	Exp [b]	Comp	Comp	Exp [b]
Bond length (Å)								
H1–N1	1.01	1.01	1.01	1.01	0.86	1.02	1.01	0.86
C1–N1	1.37	1.36	1.38	1.37	1.32	1.34	1.36	1.33
C1–O	1.30	1.28	1.37	1.26	1.26	1.31	1.26	1.22
C1–N2	1.35	1.39	1.37	1.41	1.37	1.40	1.41	1.38
N2–N3	1.47	1.38	1.41	1.36	1.36	1.38	1.37	1.35
C2–N3	1.42	1.31	1.37	1.30	1.29	1.32	1.30	1.28
C2–C3	1.42	1.47	1.45	1.49	1.49	1.51	1.49	1.49
C2–C8	1.47	1.49	1.48	1.49	1.47	1.47	1.49	1.50
C8–C9	1.43	1.42	1.42	1.42	1.38	1.42	1.41	1.36
C3–N4	1.42	1.38	1.41	1.37	1.35	1.39	1.37	1.36
N4–M	1.88	1.91	1.97	2.07	2.03	2.02	2.23	2.14
O–M	1.93	1.96	2.03	2.19	2.03	1.96	2.23	2.24
Cl–M	–	2.22	–	2.29	2.63	–	2.31	2.25
Cl'–M	–	2.82	–	2.34	2.20	–	2.36	2.24
Bond angles								
H1–N1–C1	117.35	117.14	117.31	117.23	120.08	118.25	117.12	119.78
N1–C1–O	120.09	122.23	120.09	123.06	124.11	121.10	123.36	124.48
O–C1–N2	119.17	118.99	121.91	121.40	120.07	118.55	120.32	120.83
C1–N2–N3	113.87	111.46	114.81	113.57	112.88	113.24	113.91	114.05
N2–N3–C2	116.31	126.11	122.15	125.81	124.57	128.67	123.89	122.31
N3–C2–C3	111.36	110.64	113.15	112.79	111.22	111.51	113.60	115.29
C2–C3–C4	126.21	124.59	123.39	122.77	123.90	122.14	122.97	123.39
C2–C3–N4	115.07	114.46	117.96	116.73	115.09	117.91	115.72	113.80
N3–C2–C8	122.50	123.79	122.74	124.83	124.87	125.05	124.30	124.44
C2–C8–C9	120.77	117.93	119.99	120.43	119.23	119.54	120.67	119.97
Dihedral angle (°)								
H1–N1–C1–O	5.26	5.79	3.32	4.19	0.09	1.04	3.85	0.07
H1–N1–C1–N2	-175.01	-176.21	-176.99	-176.04	177.42	-178.84	-176.79	-177.95
N1–C1–N2–N3	-164.57	-174.61	-171. 48	-178.93	171.10	-178.47	179.27	-174.46
C1–N2–N3–C2	-143.46	-173.10	-144.00	-164.72	-172.52	-168.78	-172.38	177.74
N2–N3–C2–C3	150.21	176.67	153.34	172.34	178.57	173.91	176.46	179.26
N3–C2–C3–C4	156.27	-179.02	160.03	165.89	-177.59	169.17	169.57	-176.32
N3–C2–C3–N4	-20.02	2.00	-17.33	-13.44	2.10	-8.91	-8.98	2.47
N3–C2–C8–C9	-33.95	63.03	36.69	59.80	53.29	47.11	64.45	65.16
C2–C3–N4–M	0.83	3.05	0.98	-2.17	2.08	4.92	-7.98	-1.31
N2–C1–O–M	-0.88	13.05	2.52	12.80	7.93	0.45	19.34	-10.09

[a] M= Ni²⁺, Cu²⁺ and Zn²⁺. [b] X-ray crystallographic data was taken from reference [67].

Table 4.6 Reaction energies and thermodynamic properties of the complexations of picolinaldehyde N-oxide thiosemicarbazone (Hpiotsc, $\mathbf{L^1}$) and 2-benzoyl pyridine semicarbazone (H2BzPS, $\mathbf{L^2}$) with Ni(II), Cu(II) and Zn(II)

Reactions/systems	ΔE^O [a]	ΔH^O_{298} [a]	ΔG^O_{298} [a]
Hpiotsc complexes			
$2\mathbf{L^1} + Ni^{2+} \rightarrow Ni\,\mathbf{L^1_2}^{2+,\,b}$	-495.31	-511.97	-473.13
$2\mathbf{L^1} + Cu^{2+} \rightarrow Cu\,\mathbf{L^1_2}^{2+}$	-457.49	-457.11	-436.71
$2\mathbf{L^1} + Zn^{2+} \rightarrow Zn\,\mathbf{L^1_2}^{2+}$	-415.11	-415.32	-393.06
H2BzPS complexes			
$\mathbf{L^2} + Ni^{2+} \rightarrow Ni\,\mathbf{L^2}^{2+}$	-730.80	-731.57	-720.96
$\mathbf{L^2} + Ni^{2+} + 2Cl^- \rightarrow NiL^2Cl_2$	-728.10	-729.50	-703.36
$\mathbf{L^2} + Cu^{2+} \rightarrow Cu\,\mathbf{L^2}^{2+}$	-703.38	-703.80	-694.08
$\mathbf{L^2} + Cu^{2+} + 2Cl^- \rightarrow CuL^2Cl_2^{\,,c}$	-690.15	-691.08	-666.48
$\mathbf{L^2} + Zn^{2+} \rightarrow Zn\,\mathbf{L^2}^{2+}$	-298.27	-299.21	-288.54
$\mathbf{L^2} + Zn^{2+} + 2Cl^- \rightarrow ZnL^2Cl_2^{\,,c}$	-650.93	-651.79	-627.46

[a] In kcal/mol. [b] X-ray structure is reported in reference [66]. [c] X-ray structure is reported in reference [67].

4.3 Aryl semicarbazones and QSAR analysis

The **1A'** is an isomer of the **1A** and the compound **3** is the parent structure of all the compounds **1A**, **1A'**, **1B**, **1C**, **1D**, **1E**, **2A**, **2B**, **2C**, **2D** and **2E**. The physicochemical, molecular and electronic, topological parameters of the aryl semicarbazones were used in the QSAR analysis for the antituberculous activity. The chemical structures of aryl semicarbazones and their antituberculous activities are shown in Table 4.7. The indicator variable I_1 is obviously based on the NO_2 group which is located as different substituents R_1, R_2 and R_3. The relative activities depending on the NO_2 group are in decreasing order: $R_2 > R_3 > R_1$ as shown by a compound set {**1A**, **1B**, **1C**} and {**2A**, **2B**, **2C**}. The activities of a set {**2A**, **2B**, **2C**} are respectively smaller than a set {**1A**, **1B**, **1C**} because the substituent $R_6 = NHCOCH_3$ increases the activities but double substituents $R_4 = CH_3$ and $R_5 = Cl$ decrease the activities.   Therefore, no double substitution of substituents $R_4 = CH_3$ and $R_5 = Cl$ is defined as $I_2 = 1$ and the substituent $R_6 = NHCOCH_3$ is defined as $I_3 = 1$. The effects to activities of various substituents R_1, R_2, R_3, R_4, R_5 and R_6 in the aryl semicarbazones can be roughly scored as shown in Table 4.8. These scores were therefore compiled to the indicator variables I_1, I_2 and I_3 as described in previous chapter. The indicator variable I_4 is defined as the combination of I_1, I_2 and I_3 of which distribution ratio is parametized as 2.5:1:2 respectively.

The antituberculous activity data, the physicochemical properties Log P, MR and indicator variables I_1, I_2, I_3 and I_4 of the aryl semicarbazones are given in Table 4.9. The high correlation coefficients between independent descriptors and activities of the compounds shown in Table 4.10 were used in the QSAR models. These independent descriptors are shown in Table A.1. The multiple linear regression (MLR) analysis applied using the activity (A) of the aryl semicarbazones and their independent descriptors hydrophobic coefficient Log P, I_4 and both was obtained as the following QSAR models.

Model I:

A = − 1.098 (±0.154) Log P + 4.825 (±0.356) $\hspace{4cm}$ (4.1)

n = 10; r = 0.933; r^2 = 0. 864; s = 1.067; F = 51.004; q^2 = 0.776,

Model II:

A = 0.752 (±0.085) I_4 + 0.632 (±0.476) $\hspace{4cm}$ (4.2)

n = 10; r = 0.952; r^2 = 0.906; s = 0.886; F = 77.506; q^2 = 0.726,

Model III:

A = − 0.489 (±0.209) Log P + 0.466 (±0.140) I_4 + 2.279 (±0.801) $\hspace{2cm}$ (4.3)

n = 10; r = 0.973; r^2 = 0.947; s = 0.710; F = 63.060; q^2 = 0.835,

QSAR models I, II and III are shown in equations (4.1), (4.2) and (4.3), respectively. All three models with correlation coefficients larger than 0.973 were carried out. The correlation coefficients between the observed and computed activities of the models I, II and III are 0.933 (s = 1.067), 0.952 (s = 0.886) and 0.973 (s = 0.710) as graphically shown in Figures 4.5(a), 4.5(b) and 4.5(c), respectively. As the cross-lalidation coefficient of data set of moldels I, II and III are q^2 = 0.776, 0.726 and 0.835 respectively, it obviously confirm that the model III is the most predictive model. To get high correlation with the compounds' activities, indicator variable I_4 is therefore defined as $\frac{5}{2}I_1 + I_2 + 2I_3$. Models based on the I_4 results high correlation with the activities. If the I_4 in model III can be substituted by term $\frac{5}{2}I_1 + I_2 + 2I_3$ and the Equation (4.4) will be formed. Theoretically, the Equation (4.4) must be equivalent to Equation (4.3).

A = − 0.489 (±0.209) Log P + 1.165 (±0.140) I_1 + 0.466 (±0.140) I_2

$\hspace{1cm}$ + 0.932 (±0.140) I_3 + 2.279 (±0.801) $\hspace{4cm}$ (4.4)

All regression equations, n is the number of compounds, r and r^2 are the correlation coefficient and its squared value, s is the standard error of the estimate and

F is the F-ratio between the variances of computed and observed activities. The values given in the parentheses are the standard errors of the regression coefficients.

A SQAR model of the aryl semicarbazones as anti-tuberculosis agent carried out using MLR analysis in conjunction with a partition coefficient Log P and indicator variable I_4 is represented by the model III ($r = 0.973$, see Figure 4.5) as the best model and the **1b** compound is an outlier (see Table 4.11).

The antituberculous activity sequences in decreasing order of 10 aryl semicarbazones obtained from the measurement and the model III are 1B > 1C > 1A > 2B > 2C > 2A > 1D > 1E > 2D = 2E and 1B > 1C > 1A > 2B > 2C > 2A > 1D > 1E > 2D > 2E, respectively. This shows that the model III shows very good correlation between structure and activity of the aryl semicarbazones, although the model was generated from the small number of the aryl semicarbazone derivatives.

The predicted activities of the parent compound **3** are 1.344, 1.384 and 1.195 for the models I, II and III, respectively. The predicted activities of the simulated compounds **4A**, **4B**, **4C**, **4D** and **4E** using the model III are 2.550, 4.880, 3.715, 0.00 (-0.398) and 0.00 (-0.666), respectively. These simulated compounds may not be easy to synthesize due to their functionalizations. However, these predicted biological activities are helpful for making decision to synthesize these compounds as the anti-tuberculosis agent.

Table 4.7 Chemical structures of aryl semicarbazones and antituberculous activity

Compound	R_1	R_2	R_3	R_4	R_5	R_6	Activity [a]
1A	NO_2	H	H	H	H	$NHCOCH_3$	5.691
1B	H	NO_2	H	H	H	$NHCOCH_3$	9.125
1C	H	H	NO_2	H	H	$NHCOCH_3$	6.016
1D	OH	H	H	H	H	$NHCOCH_3$	3.419
1E	H	H	$N(CH_3)_2$	H	H	$NHCOCH_3$	3.046
2A	NO_2	H	H	CH_3	Cl	H	3.772
2B	H	NO_2	H	CH_3	Cl	H	4.866
2C	H	H	NO_2	CH_3	Cl	H	4.226
2D	OH	H	H	CH_3	Cl	H	0.000
2E	H	H	$N(CH_3)_2$	CH_3	Cl	H	0.000
3	H	H	H	H	H	H	- [b]

[a] Derived from the biological testing data Reference 35 and computed using an Equation 3.1, Reference 43. [b] No measurement.

Table 4.8 The effect to activities of the functional groups for various substituents R_1, R_2, R_3, R_4, R_5 and R_6 on the aryl semicarbazones

Group (substituent)	Effect to activity [a]
NO_2 (R_1)	+
NO_2 (R_2)	+++
NO_2 (R_3)	++
$NHCOCH_3$ (R_6)	++
CH_3 (R_4)+ Cl (R_5)	– –
OH (R_1)	±
$N(CH_3)_2$ (R_3)	±

[a] +, ++, +++ are the small, medium and high effects, respectively, – – is the negative effect and ± is no effect.

Table 4.9 Activity and indicator variables of the aryl semicarbazones

Compounds	Activity [a]	I_1 [b]	I_2 [c]	I_3 [d]	I_4 [e]
1A	5.691	1	1	1	5.5
1B	9.125	3	1	1	10.5
1C	6.016	2	1	1	8.0
1D	3.419	0	1	1	3.0
1E	3.046	0	1	1	3.0
2A	3.772	1	0	0	2.5
2B	4.866	3	0	0	7.5
2C	4.226	2	0	0	5.0
2D	0.000	0	0	0	0.0
2E	0.000	0	0	0	0.0
3	- [f]	0	1	0	1.0

[a] Computed from Eqaution 3.1. [b - e] Defined in section 3.2.2. [f] No measurement.

Table 4.10 Correlation (r^2) matrix of the aryl semicarbazones

	Activity	I_1	I_2	I_3	I_4	log P	MR	μ	E_{HOMO}	E_{LUMO}
Activity	1.000									
I_1	0.615	1.000								
I_2	0.310	0.000	1.000							
I_3	0.310	0.000	1.000	1.000						
I_4	0.821	0.790	0.209	0.318	1.000					
log P	0.865	0.534	0.236	0.236	0.762	1.000				
MR	0.001	0.026	0.134	0.134	0.000	0.004	1.000			
μ	0.101	0.421	0.088	0.088	0.194	0.149	0.064	1.000		
E_{HOMO}	0.011	0.291	0.475	0.475	0.027	0.043	0.342	0.287	1.000	
E_{LUMO}	0.216	0.082	0.082	0.082	0.148	0.263	0.246	0.008	0.058	1.000

Table 4.11 Observed and predicted activities of the aryl semicarbazones computed via three models

Compound	Observed	Model I		Model II		Model III	
		Predicted	Residual	Predicted	Residual	Predicted	Residual
1a	5.692	6.902	-1.211	4.768	0.923	5.767	-0.076
1b	9.125	6.902	2.223	8.528	0.597	8.097	1.028
1c	6.016	6.902	-0.886	6.648	-0.632	6.932	-0.916
1d	3.420	2.921	0.498	2.888	0.531	2.829	0.590
1e	3.045	2.318	0.728	2.888	0.158	2.561	0.485
2a	3.772	4.557	-0.785	2.512	1.260	3.325	0.447
2b	4.866	4.557	0.309	6.272	-1.406	5.655	-0.789
2c	4.226	4.557	-0.331	4.392	-0.166	4.490	-0.264
2d	0.000	0.575	-0.575	0.632	-0.632	0.386	-0.386
2e	0.000	-0.028	0.028	0.632	-0.632	0.118	-0.118
3	-	1.344	-	1.384	-	1.195	-

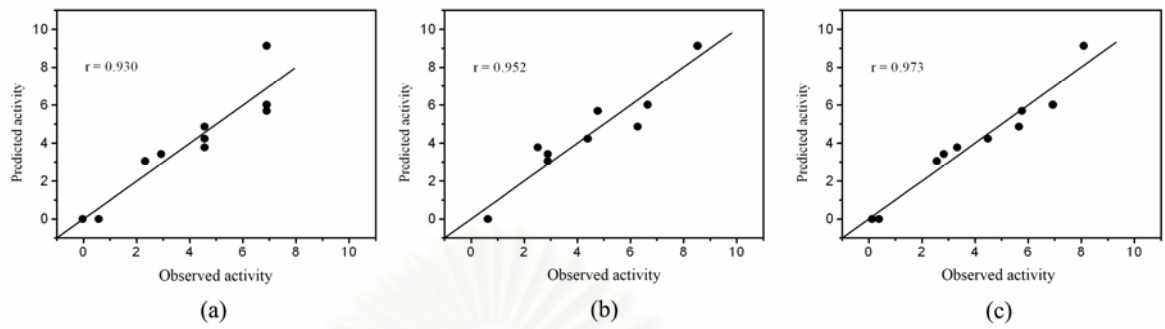**Figure 4.5** Correlation plots between observed and predicted activities using (a) model I, (b) model II and (c) model III.

CHAPTER V

CONCLUSIONS

The sytems of picolinaldehyde N-oxide thiosemicarbazone (Hpiotsc) and 2-benzoylpyridine semicarbazone (H2BzPS), their structures optimizations at the B3LYP/LANL2DZ level, determinations of enegies and thermodynamic properties of their tautomerizations were carried out. The B3LYP/LANL2DZ-optimized structures of HPiotsc, H2BzPS complexes with Ni(II), Cu(II) and Zn(II) and thermodynamic properties of their complexations in gas and aqueous phases were theoretically obtained.

For the aryl semicarbazones, descriptors used in the QSAR study based on the AM1-optimized structures of are fairly good. A SQAR analysis of a novel class of anti-tuberculosis agent was carried out using MLR analysis in conjunction with the octanol-water partition coefficient and the indicator variables. Due to the QSAR study of ten compounds of the aryl semicarbazones, the most reliable QSAR model for the antituberculous activities of the aryl semicarbazones is a function of the partition coefficient and indicator variable I_4. No test set of the aryl semicarbazones has been examined but the activities of the simulated compounds **4A, 4B, 4C, 4D** and **4E** were predicted.

REFERENCES

[1]   V.M. Kolb, J.W. Stupar, T.E. Janota, W.L. Duax, J. Org. Chem. 54 (1989) 2341.

[2]   J.R. Dimmock, J.M. McColl, S.L. Wonko, R.S. Thayer, D.S. Hancock, J. Med. Chem. 26 (1991) 529.

[3]   J.R. Dimmock, K.K. Sidhu, R.S. Thayer, P. Mack, M.J. Duffy, R.S. Reid, J.W. Quail, U. Pugazhenthi, A. Ong, J.A. Bikker, D.F. Weaver, J. Med. Chem. 36 (1993) 2243.

[4]   J.R. Dimmock, S.N. Pandeya, J.W. Quail, U. Pugazhenthi, T.M. Allen, G.Y. Kao, J. Balzarini, E. DeClercq, J. Med. Chem. 30 (1995) 303.

[5]   Y.P. Tian, C.Y. Duan, Z.L. Lu, X.Z. You, Polyhedron 15 (1996) 2263.

[6]   L. Bresolin, R.A. Burrow, M. Hörner, E. Bermejo, A. Castiñeiras, Polyhedron 16 (1997) 3947.

[7]   F. Basuli, M. Ruf, C.G. Pierpont, S. Bhattacharya, Inorg. Chem. 37 (1998) 6113.

[8]   F. Basuli, S.M. Peng, S. Bhattacharya, Inorg. Chem. 39 (2000) 1120.

[9]   F. Basuli, S.M. Peng, S. Bhattacharya, Inorg. Chem. 40 (2001) 1126.

[10]   P. Gupta, F. Basuli, S.M. Peng, G.H. Lee, S. Bhattacharya, Inorg. Chem. 42 (2003) 2069.

[11]   I. Pal, S. Dutta, F. Basuli, S. Goverdhan, S.M. Peng, G.H. Lee, S. Bhattacharya, Inorg. Chem. 42 (2003) 4338.

[12]   G.F. de Sousa, V.M. Deflon, E. Niquet, J. Mol. Struct. 687 (2004) 17.

[13]   N.C. Kasuga, K. Sekino, C. Koumo, N. Shimada, M. Ishikawa, K. Nomiya, J Inorg. Biochem. 84 (2001) 55.

[14]   L.H. Hall, S.Y. Chen, B.J. Barnes, D.X. West, Metal Based Drugs 6 (1999) 143.

[15]   E. Bermejo, R. Carballo, A. Castineiras, R. Dominguez, A.E. Liberta, C. Maichle-Mossmer, D.X. West , Z. Naturforsch. B 54 (1999) 777.

[16]   J.M. Perez, A.I. Matesanz, A. Marin-Ambite, P. Navarro, C. Alonso, P. Souza, J. Inorg. Biochem. 75 (1999) 255.

[17]   K.H. Reddy, P.S. Reddy, P.R. Babu, J. Inorg. Biochem. 77 (1999) 169.

[18]   P.F. Kelly, A.M.Z. Slawin, A. Soriano-Rama, J. Chem. Soc. Dalton Trans. (1996) 53.

[19] D.X. West, S.B. Padhye, P.B. Sonawane, Structure Bonding 76 (1991) 1.

[20] A.E. Liberta, D.X. West, Biometal. 5 (1992) 121.

[21] D.X. West, A.E. Liberta, S.B. Padhye, R.C. Chikate, P.B. Sonawane, A.S. Kumbhar, R.G. Yerande, Coord. Chem. Rev. 123 (1993) 49.

[22] U. Abram, K. Ortner, R. Gust, K. Sommer, J. Chem. Soc. Dalton Trans. (2000) 735.

[23] D.X. West, G.A. Bain, R.J. Butcher, J.P. Jasinski, Y. Li, R.Y. Pozdniakiv, J. Valdes-Martinez, R.A. Toscano, S. Hernandes-Ortega, Polyhedron 15 (1996) 665.

[24] R.R. Babu, N. Vijayan, R. Gopalakrishnan, P. Rramasamy, J. Crystal. Growth 240 (2002) 545.

[25] V. Ruangpornvisuti, K. Supakornchailert, C. Tungchitpienchai, B. Wanno, Struct. Chem. 17 (2006) 27.

[26] V. Ruangpornvisuti, B. Pulpoka, T. Tuntulani, K. Thipyapong, C. Suksai, Bull. Korean Chem. Soc. 23 (2002) 555.

[27] K. Thipyapong, Y. Arano, V. Ruangpornvisuti, J. Mol. Struct. (Theochem) 676 (2004) 65.

[28] K. Thipyapong, N. Yasarawan, B. Wanno, Y. Arano, V. Ruangpornvisuti, J. Mol. Struct. (Theochem) 755 (2005) 45.

[29] C. M. Shoen, M. S. DeStefano, M. R. Sklaney, B. J. Monica, A. M. Slee, M. H. Cynamon, J. Antimicrob. Chemother. 53 (2004) 641.

[30] C. Dye, S. Scheele, P. Dolin, JAMA 282 (1999) 677.

[31] B. R. Bloom, C. J. Murray, Science 257 (1992) 1055.

[32] M. D. Iseman, New Engl. J. Med. 329 (1993) 784.

[33] A. Nayyar, A. Malde, R. Jain, E. Coutinho, Bioorg. Med. Chem. 14 (2006) 847-856.

[34] P.Yogeeswari, D. Sriram, A. Brahmandam, I .Sridharan, R. Thirumurugan, J. P. Stables, Med. Chem. Res., 12 (2003) 57-68.

[35] D. J. Sriram, P. Yogeeswari, R. Thirumurugan, Bioorg. Med. Chem. Lett. 14 (2004) 3923.

[36] S. Vangapandu, M. Jain, R. Jain, S. Kaur, P. Singh, Bioorg. Med. Chem. 12 (2004) 2501.

[37] B. Vaitilingam, A. Nayyar, P. Palde, V. Monga, R. Jain, S. Kaur, P. Singh, Bioorg. Med. Chem. 12 (2004) 4179.

[38] V. Monga, A. Nayyar, B. Vaitilingam, P. Palde, S. Jhamb, S. Kaur, P. Singh, R. Jain, Bioorg. Med. Chem. 12 (2004) 6465.

[39] S. Dutta, S. Padhye, K. Indira Priyadarsini, C. Newton, Bioorg. Med. Chem. Lett. 15 (2005) 2738.

[40] V. Ruangpornvisuti, W. Banchob, J. Mol. Model. 10 (2004) 418.

[41] C. Hansch, P.P. Maloney, T. Fujita, R.M. Muir, Nature 194 (1962) 178.

[42] C. Hansch, T. Fujita, J. Am. Chem. Soc. 86 (1964) 1616.

[43] CoMFA and QSAR Manual, Sybyl 7.0, Associates Inc., 1699 S Hanley Rd., St. Louis, MO 631444, USA.

[44] M.J.S. Dewar, C.H. Reynolds, J. Comp. Chem. 2 (1986) 140.

[45] J. J. P. Stewart, J. Comp. Chem. 10 (1989) 209.

[46] A.D. Becke, Phys Rev A 38 (1988) 3098.

[47] C. Lee, W. Yang, R.G. Parr, Phys. Rev. B 37 (1988) 785.

[48] A.D. Becke, Chem. Phys. 98 (1993) 5648.

[49] P.J. Hay, W.R. Wadt, J. Chem. Phys. 82(1985) 270.

[50] W.R. Wadt, P.J. Hay, J. Chem. Phys. 82(1985) 284.

[51] P.J. Hay, W.R. Wadt, J. Chem. Phys. 82(1985) 299.

[52] M. Cossi, N. Rega, G. Scalmani, V. Barone, J. Comput. Chem. 24 (2003) 669.

[53] E. Cancès, B. Mennucci, J. Tomasi, J. Chem. Phys. 107 (1997) 3032.

[54] M. J. Frisch, G. W. Trucks, H. B. Schlegel, G. E. Scuseria, M. A. Robb, J. R. Cheeseman, V. G. Zakrzewski, J. A. Montgomery, Jr., R. E. Stratmann, J. C. Burant, S. Dapprich, J. M. Millam, A. D. Daniels, K. N. Kudin, M. C. Strain, O. Farkas, J. Tomasi, V. Barone, M. Cossi, R. Cammi, B. Mennucci, C. Pomelli, C. Adamo, S. Clifford, J. Ochterski, G. A. Petersson, P. Y. Ayala, Q. Cui, K. Morokuma, D. K. Malick, A. D. Rabuck, K. Raghavachari, J. B. Foresman, J. Cioslowski, J. V. Ortiz, A. G. Baboul, B. B. Stefanov, G. Liu, A. Liashenko, P. Piskorz, I. Komaromi, R. Gomperts, R. L. Martin, D. J. Fox, T. Keith, M. A. Al-

Laham, C. Y. Peng, A. Nanayakkara, C. Gonzalez, M. Challacombe, P. M. W. Gill, B. Johnson, W. Chen, M. W. Wong, J. L. Andres, C. Gonzalez, M. Head-Gordon, E. S. Replogle, and J. A. Pople, Gaussian 03, Gaussian, Inc., Pittsburgh PA, 2003.

[55] P. Flükiger, H.P. Lüthi, S. Portmann, J. Weber, MOLEKEL 4.3: Swiss Center for Scientific Computing, Manno (Switzerland), 2000.

[56] J.R. Sabin, S.B Trickey, S.P. Apell, J. Oddershede, Int. J. Quantum Chem. 77 (2000) 358.

[57] T. Koopmans, Physica. 1 (1933) 104.

[58] E. Lewars, Computational chemistry: Introduction to the Theory and Applications of Molecular and Quantum Mechanics, Kluwer Academic Publishers, Boston, 2003.

[59] B. Wanno, V. Ruangpornvisuti, J. Mol. Struct. (Theochem) 766 (2006) 159.

[60] HyperChem 7.0, Tools for Molecular Modeling, Hypercube, 2005.

[61] Chem3D Ultra 9.0, Molecular Modeling and Analysis, CambridgeSoft, 2005.

[62] CAChe 6.1, Modeling Software, Cache Group, Fujitsu, 2005.

[63] P.R. Verma, A. Kurup, C. Hansch, Bioorg. Med. Chem. 13 (2005) 237.

[64] P.R. Verma, A. Kurup, S. B. Merapati, C. Hansch, Bioorg. Med. Chem. 13 (2005) 933.

[65] P.R. Verma, C. Hansch, Bioorg. Med. Chem. 13 (2005) 2355.

[66] A. Pérez-Rebolledo, O.E. Piro, E.E. Castellano, L.R. Teixeira, A.A. Batista, H. Beraldo, J. Mol. Struct. 794 (2006) 18.

[67] Y. Qing, D.J. Hua, Z.L. Gang, Z.X. Qing, B.H. Dong, L. Hong, J. Mol. Struct. 794 (2006) 71.

APPENDICES

Table A.1 Aryl semicarbazones, their antituberculous activity and indicator
parameters

Compound	Activity [a]	I_4 [b]	Log P	MR	μ [c]	E_{HOMO} [d]	E_{LUMO} [d]	$E_{HOMO\text{-}LUMO}$ [d]
1A	5.691	3.5	-1.892	90.326	3.574	-8.497	-1.217	7.28
1B	9.125	4.5	-1.892	90.326	6.031	-8.609	-1.099	7.51
1C	6.016	4.0	-1.892	90.326	7.316	-8.639	-1.326	7.31
1D	3.419	2.5	1.734	85.699	1.993	-8.387	-2.382	6.01
1E	3.046	2.5	2.283	98.434	1.761	-8.129	-0.051	8.08
2A	3.772	1.0	0.244	87.09	4.091	-9.49	-1.247	8.24
2B	4.866	2.0	0.244	87.09	4.887	-9.579	-1.13	8.45
2C	4.226	1.5	0.244	87.09	8.45	-9.624	-1.359	8.27
2D	0.000	0.0	3.871	82.463	4.677	-8.861	-0.273	8.59
Tested compounds								
3	2.550 [e]	4.5	-0.927	- [f]	- [f]	- [f]	- [f]	- [f]
4A	4.880 [e]	9.5	-0.927	- [f]	- [f]	- [f]	- [f]	- [f]
4B	3.715 [e]	7	-0.927	- [f]	- [f]	- [f]	- [f]	- [f]
4C	-0.398 [e]	2	2.720	- [f]	- [f]	- [f]	- [f]	- [f]
4D	-0.666 [e]	2	3.268	- [f]	- [f]	- [f]	- [f]	- [f]
4E	2.550 [e]	4.5	-0.927	- [f]	- [f]	- [f]	- [f]	- [f]

[a] Computed using Equation (3.1). [b] Defined as $\frac{5}{2}I_1 + I_2 + 2\,I_3$. [c] In debye. [d] In eV.
[e] Predicted activities. [f] No calculation.